

The sensitivity of the Atlantic meridional overturning circulation to enhanced freshwater discharge along the entire, eastern and western coast of Greenland

Lei Yu^{1,4} · Yongqi Gao^{2,4} · Odd Helge Otterå³

Received: 4 December 2014 / Accepted: 9 May 2015 / Published online: 28 May 2015
© Springer-Verlag Berlin Heidelberg 2015

Abstract The possible responses of the Atlantic meridional overturning circulation (AMOC) to increased freshwater discharge along the Greenland coast has become an issue of growing concern given the increasing rate of the Greenland ice sheet (GrIS) melting. A recent model study suggested a weakened AMOC of about 13–30 % when a freshwater anomaly of 0.1 Sv ($1 \text{ Sv} = 10^6 \text{ m}^3 \text{ s}^{-1}$) was released along the entire Greenland coast during the late twentieth century (1965–2000). In this study we use a fully coupled climate model to examine the sensitivity of AMOC to a similar amount of freshwater forcing, but released separately along the eastern, the western and the entire Greenland coast. Our results show that in all three cases there is a general weakening of the AMOC mainly due to a reduced formation of Labrador Sea Water. Moreover, when additional freshwater is released along the eastern coast of Greenland, the AMOC weakens more compared to the other two cases. The different degree of convective mixing reduction in the Irminger Sea is the main reason for the spread in AMOC responses in the three freshwater-hosing experiments. Compared to the other two experiments, the eastern-coast experiment shows a relative warming in the

Labrador Sea and the generation of a negative Greenland tip jet-like wind-pattern anomaly. These anomalies lead to a weaker convective mixing in the southern Irminger Sea, and result subsequently in less formation of the simulated Upper Labrador Sea Water (ULSW) in the eastern coast experiment. This study therefore highlights a potential important role for ULSW formation in determining the sensitivity of the AMOC in response to large GrIS melting.

Keywords AMOC · Greenland ice sheet melting · Freshwater-hosing experiment · Upper Labrador Sea water formation

1 Introduction

The Atlantic meridional overturning circulation (AMOC) is an active component of the global climate system (Boyle and Keigwin 1987; Broecker 1991; Manabe and Stouffer 1999; Rahmstorf 1994; Rahmstorf and Ganopolski 1999). It transports large amounts of heat with the Gulf Stream and North Atlantic Current from the tropical and subtropical oceans to the North Atlantic. Here the North Atlantic Current splits into two branches: The first branch is the western branch with southwestward circulation, which includes a mix of fresh and cold polar water from the east-coast of Greenland and the Canadian Archipelago. This branch is part of the cyclonic circulation of the North Atlantic sub-polar gyre (Langehaug et al. 2012). The second branch is the eastern branch, which carries heat poleward into the Nordic Seas (the Greenland, the Iceland and the Norwegian Seas) through the Greenland-Scotland Ridge (GSR). In winter, the North Atlantic Current releases heat to the overlying atmosphere, which leads to strong winter convective mixing in the Labrador/Irminger Seas and formation of

✉ Lei Yu
yulei@mail.iap.ac.cn

¹ Climate Changes Research Center, Institute of Atmospheric Physics, Chinese Academy of Sciences, Beijing 100029, China

² Nansen Environmental and Remote Sensing Center/Bjerknes Center for Climate Research, Bergen, Norway

³ Uni Research Climate and Bjerknes Centre for Climate Research, Bergen, Norway

⁴ Nansen-Zhu International Research Centre, Institute of Atmospheric Physics, Chinese Academy of Sciences, Beijing 100029, People's Republic of China

subpolar intermediate-deep waters. These subpolar intermediate-deep waters together with the cold and dense southward overflowing deep water from the Nordic Seas feeds the lower limb of the AMOC, known as the North Atlantic Deep Water (NADW).

The perturbation in the freshwater forcing can modify the stability of the water column through the changes in the surface buoyancy. Early modeling studies have suggested that the surface freshening can increase the buoyancy, stabilize upper ocean layers and thus weaken the rate of deep water formation (e.g. Stommel 1961; Zhang et al. 1999; Mohammad and Nilsson 2004; Otterå et al. 2004; Yu et al. 2008). This subsequently leads to a slow-down of the AMOC (e.g. Stommel 1961; Rooth 1982; Bryan 1986; Rahmstorf 1996; Tziperman 2000). Motivated by paleo records documenting numerous large freshwater events and recent observations of Arctic river runoff (e.g., Manabe and Stouffer 1995; Peterson et al. 2002; Dickson et al. 2002; Rignot et al. 2011; Giles et al. 2012; Smeed et al. 2014), numerical studies have been performed to investigate the impacts of various freshwater perturbations in the northern high latitudes on the AMOC and the associated climate changes (e.g. Manabe and Stouffer 1997; Schiller et al. 1997; Vellinga et al. 2002; Stouffer et al. 2006; Jungclauss et al. 2006; Yu et al. 2009; Zhang et al. 2010; Bakker et al. 2012; Swingedouw et al. 2013; Weijer et al. 2012; Blaschek et al. 2015). A robust finding from these earlier studies is that the AMOC reduces if there is a net flux of freshwater added to the northern high latitudes. While the models generally agree on the sign of the AMOC change induced by the additional freshwater forcing, they show quite a large spread in terms of how sensitive the AMOC is to freshwater forcing. For example, Stouffer et al. (2006) reported a quite large range of estimated sensitivities of the AMOC in response to additional freshwater input. The simulated AMOC weakening varies between around 10–60 % after 100 years for a typical freshwater-hosing experiments where 0.1 Sv ($1 \text{ Sv} = 10^6 \text{ m}^3 \text{ s}^{-1}$) of freshwater is added uniformly to a latitudinal band (50–70°N) in the North Atlantic. Some reasons for the uncertainty in the simulated AMOC responses have been proposed. Weijer et al. (2012) compared the transient response of simulated AMOC to 0.1 Sv of freshwater forcing around Greenland in a eddy-resolving (grid spacing of 0.1°) with response in a lower-resolution ocean model. Their results show that the declining in AMOC is more persistent in the eddy-resolving configuration. Toom et al. (2014) showed that an additional freshwater perturbations of 0.5 Sv led to a quantitatively comparable reduction of the AMOC between eddy-resolving and non-eddy versions of POP. Swingedouw et al. (2013) showed that reductions of AMOC were weaker in climate models coupled with fine-resolution ocean models than those in climate models coupled with

coarse-resolution ocean models. One of the reasons for this is that the fine-resolution ocean models allow the additional freshwater to escape from the subpolar gyre. Furthermore, the simulated AMOC responses to freshwater perturbations are also dependent on the ocean mixing schemes and convection parametrizations that are used in models (i.e. Gao et al. 2003; Nilsson et al. 2003; Marzeion et al. 2007). For example, it has been suggested that the stratification-dependent mixing may increase the sensitivity of the AMOC to surface freshwater fluxes (Marzeion and Levermann 2009), and a similar result was also obtained in a coupled model (Yu et al. 2008). Finally, it has been shown that different model parametrizations could lead to different responses of AMOC to low and high GrIS melting rates under past as well as future climate backgrounds (Blaschek et al. 2015).

Model studies suggest that the response of AMOC to a given freshwater input into a region is highly non-uniform and differs greatly among the climate models. In addition, the simulated AMOCs have also been shown to be sensitive to the location where the freshwater is released from. For example, Smith and Gregory (2009) added 0.5 Sv of freshwater to 11 different latitudinal bands (from 35 to 75°N) within the North Atlantic and Arctic Ocean in a fully-coupled climate model, and found that the declines in the AMOC strength differed substantially among the various experiments. In their results the largest reduction of the AMOC was found when the region of deepwater formation was forced directly. Recently the impact of freshwater discharge along more realistic regions (rather than the large latitudinal bands) on AMOC and associated climate changes have been investigated. For example, Saenko et al. (2007) investigated the impact of more localized freshwater perturbations (the south-east coast of Greenland versus the north-east coast of North America), showing the potential important role of local air-sea interaction on the North Atlantic climate. Roche et al. (2010) performed various freshwater perturbation experiments under a simulated Last Glacial Maximum (LGM) climate state using an Earth system model. The freshwater was discharged to regions that are believed to be places of iceberg melting or river outlets draining the melting ice sheets during the LGM. Their results suggested that the AMOC was most sensitive when the freshwater pulse was added to the main deep water formation zones.

Recently an increase in the Greenland ice mass losses has been reported (e.g., Chen et al. 2006; Thomas et al. 2009; Fettweis et al. 2011; Rignot et al. 2011; Shepherd et al. 2012). For example, Rignot et al. (2011) estimated the acceleration rate of GrIS loss to be about 20 Gt year^{-2} over the period 1993–2011; Shepherd et al. (2012) reported GrIS melting rate has increased from around 83 Gt year^{-1} (Gigatonnes per year, $1 \text{ Gt year}^{-1} = 2.8 \times 10^{-3} \text{ mm}$

$\text{year}^{-1} = 3.17 \times 10^{-5} \text{ Sv}$) over the period 1993–2003 to around 263 Gt year^{-1} over the period 2005–2010 based on reconciled ice-sheet mass balance data. Persistent ice loss from Greenland could increase the freshwater input into the North Atlantic. A recent study argues that the cumulative freshwater anomaly discharge from the GrIS since 1995 amounts to a third of the magnitude of the Great Salinity Anomaly (GSA) of the 1970s in the North Atlantic (Bamber et al. 2012). Should the GrIS melting trend continue into the future the freshwater discharge might soon exceed that of the GSA and start affecting the AMOC.

The transient responses of AMOC to GrIS melting under the present-day climate background have received a lot of attention. A recent multi-model inter-comparison study has shown a range of about 13–30 % of weakening of the AMOC during four decades in the late twentieth century (1965–2000) if an additional 0.1 Sv of freshwater is uniformly released along the entire Greenland coast (Swingedouw et al. 2013). However, the simulated spatial patterns of the GrIS melting varied considerably among the models (e.g. Mikolajewicz et al. 2007; Vizcaíno et al. 2010). Observations also show a substantial melting of western Greenland glaciers (Rignot et al. 2010) or glacier retreat under the warming waters in the East Greenland fjord (Straneo et al. 2010; Christoffersen et al. 2011, Sciascia et al. 2013). In this study we investigate and compare the sensitivities of the AMOC to additional freshwater inputs along the entire, eastern and western coasts of Greenland under the present-day climate background. The aims of this study are (1) to estimate the sensitivities of AMOC to the GrIS melting along different coasts of Greenland, and (2) to investigate the mechanisms giving rise to potential different sensitivities of AMOC to various freshwater hosing locations.

This paper is organized as follows: Sect. 2 contains descriptions of the climate model, freshwater hosing experiments and statistical methods used in this study. In Sect. 3 we present the responses of the AMOC in the three freshwater hosing experiments, and explain why responses are potentially different. The results are further discussed in Sect. 4. Finally, we end the paper with a summary and some concluding remarks in Sect. 5.

2 Descriptions of model and experiment design

2.1 Model description

The climate model used in this study is an updated version of the Bergen Climate Model (BCM2) (Otterå et al. 2009), a global, coupled atmosphere–ocean–sea-ice general circulation model (GCM). The atmosphere component is the spectral atmospheric GCM ARPEGE (Déqué et al. 1994). In this study, ARPEGE is run with a truncation at

wave number 63 (TL63), and a time step of 1800 s. All the physics and the treatment of model nonlinear terms require spectral transforms to a Gaussian grid. The physical parameterization is divided into several explicit schemes, each calculating the flux of mass, energy and/or momentum due to a specific physical process (Furevik et al. 2003).

The ocean component is Miami Isopycnic Coordinate Ocean Model (MICOM, Bleck et al. 1992). In this study, the MICOM is configured with 34 isopycnic layers below the non-isopycnic mixed layer. The horizontal ocean grid is almost regular (2.4° latitude \times 2.4° longitude). To better resolve tropical dynamics, the latitudinal grid spacing is gradually reduced to 0.8° near the equator. The vertical coordinate is the potential density with reference pressure at 2000 dbar (σ_2 -coordinate), ranging from $\sigma_2 = 30.119 \text{ kg m}^{-3}$ to $\sigma_2 = 37.800 \text{ kg m}^{-3}$.

The sea-ice model in the BCM2 is GELATO, a dynamic-thermodynamic sea-ice model that includes multiple ice categories (Salas-Méllia 2002). The OASIS (version 2) coupler (Terray et al. 1995) is used to couple the atmosphere and ocean models. For more details, please refer to Otterå et al. (2009).

Some of the improvements in the atmospheric component, ARPEGE, compared to earlier versions of BCM are: (1) an improved first order eddy-viscosity scheme for vertical diffusion in the atmospheric component (Louis 1979; Geleyn 1988) and (2) an updated turbulence scheme, which adds a limitation to the Richardson number. These improvements have contributed to removing a persistent cold bias in the global air temperature (Otterå et al. 2009). For the oceanic component (MICOM), the drift in sea surface temperatures and salinities are considerably reduced compared to previous version of BCM by applying improved conservation properties in the ocean model. Furthermore, by choosing a reference pressure at 2000 m and including thermobaric effects in the ocean model, a more realistic AMOC is simulated (Medhaug et al. 2012).

The diapycnal mixing is parameterized following McDougall and Dewar (1998) and is dependent on the local stability (background diffusivity). To incorporate shear instability and gravity current mixing, a Richardson number dependent diffusivity has been added to the background diffusivity. This stratification-dependent mixing scheme has greatly improved the water mass characteristics downstream of overflow regions (Otterå et al. 2009; Langehaug et al. 2012).

2.2 Experiment design

The basis for our freshwater hosing experiments is the present-day climatic state as simulated by a 150-year (1850–1999) all-forcing run with the BCM2 (Otterå et al. 2010; Suo et al. 2013). The external forcings include the

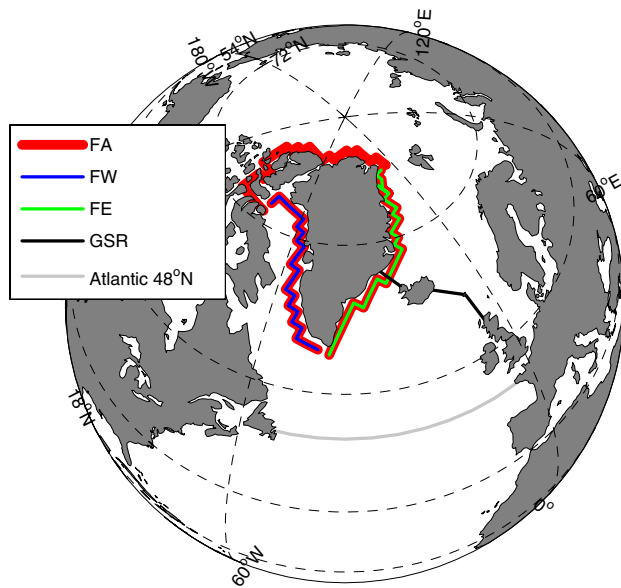


Fig. 1 The all (**bold red**), western (**green**) and eastern (**blue**) coast of the Greenland along which the additional 0.1 Sv of freshwater is released in FA, FE and FW. Additionally the GSR (**black**) and latitudinal section of 48°N (**gray**) within the Atlantic Ocean are shown

time-varying greenhouse gas concentrations, aerosol composition in the atmosphere and solar and volcanic forcings. In this study we refer to this all-forcing run as CTL since it constitutes the basis for our freshwater hosing experiments. There is not any additional freshwater input in the CTL simulation. Three freshwater-hosing experiments are performed by uniformly and continuously adding an additional 0.1 Sv freshwater along the entire (FA), the eastern (FE) and the western (FW) coasts (Fig. 1), respectively. The freshwater-hosing experiments were started from year 1965 of CTL and continue to 1999. A multi-model study (Swingedouw et al. 2013) has discussed the decadal fingerprints of the 0.1 Sv of freshwater added to the entire Greenland coast during the period 1965–1999. This study extends their study to investigate the responses of AMOC to the freshwater applied along the eastern and western coasts of Greenland. The estimate of 0.1 Sv of freshwater is partly motivated from independent coupled ice sheet-earth system model studies (Ridley et al. 2005; Mikolajewicz et al. 2007; Vizcaíno et al. 2010) showing similar melting rates under strong warming conditions for the coming centuries. It should be noted, however, that a choice of 0.1 Sv very likely overestimates the projected GrIS melting and should be regarded as an extreme choice. Therefore, the presented freshwater-hosing experiments should be viewed as sensitivity experiments only.

In this study, the term “anomalies” means the anomalies in each experiment relative to the CTL. The term “difference” means the results obtained by taking $FE - FW$, $FE - FA$ and $FW - FA$, respectively.

2.3 The method of significance examination

In order to focus on the decadal evolution of the differences in AMOC strength and the NADW formation in the three experiments, time series of difference in AMOC strength have been low-pass filtered using a 9-year-running-mean filter. Due to this, the effective degree of freedom is reduced, which must be considered when estimating statistical significance. In this study, this is solved by examining the significance of the low-pass filtered time series of the difference in AMOC using a Monte Carlo test. In the following the Monte Carlo processes is described for the comparison of the AMOC strength in the FE and the FW experiments. Firstly, we generate two random sequences from the annual time series of the AMOC strength in FE and FW. Secondly, we apply a 9-year low-pass-filter on them. In the third step we calculate the difference between the two time series. These three steps are repeated 10,000 times, and all the computed differences are sorted in ascending order. Finally, we choose the range outside the 5th and 95th percentiles of all the computed differences as the confidence range. This then ultimately determines the significance of the difference between the two compared experiments.

Meanwhile, it is necessary to determine if the presented low-pass filtered evolution of the differences is forced, or if it is just representing the unforced inherent variability in the model. In order to provide an estimate the intrinsic variability in the model, we analyze an unforced 600-year pre-industrial control with BCM (Otterå et al. 2009, hereafter referred to as CTL0). From this simulation, we pick 565 non-repetitive segments using a running 35-year window. The trend and mean value of each of our freshwater-hosing experiments are then compared against these CTL0 segments. Following Franzke (2011), if the examined trend is outside the 5th or 95th percentile of the trend ranges computed from the ensemble of CTL0 segments, we infer that the trend is statistically significant and is unlikely to have arisen from climate noise. The described method is also applied to examine the low-pass filtered decadal variability of the AMOC and NADW in each experiment.

For the spatial differences and anomalies in the physical 2d-fields, we use annual mean values without low-pass filtering. A standard t test is therefore used to examine the significance. The degree of the freedom (dof) is estimated directly by $(N1 + N2 - 2)$. Furthermore in order to exclude the representation of the inherent climate variability, we also compute the 5th and 95th percentiles of the annual climate variability from the unforced 600-year CTL0 at each grid. Only the difference at each grid point that is outside the range of 5th and 95th percentiles based on CTL0, and has significance greater than the 95 % confidence level based on t test, is estimated to be significant. Finally, in this study

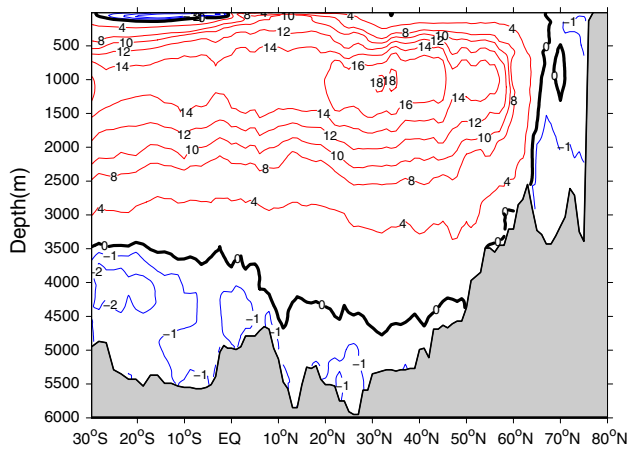


Fig. 2 The simulated long-term annual mean of meridional stream function in the Atlantic basin in CTL (averaged over the whole 150-year integration)

annual values are used whereas the winter values are used for convection and heat exchange between the ocean and atmosphere.

3 Results

3.1 The responses of the AMOC in the freshwater experiments

The simulated annual mean of the Atlantic meridional stream function in CTL (averaged over the whole 150-year

of integration) is shown in Fig. 2. The main structure of the stream function is a clockwise (positive) circulation transporting water northward from the surface to 800–1000 m. The water sinks around 60°N, and then returns southward at depths of 1500–3000 m. Below 4000 m one can see a relative weak anti-clockwise (negative) circulation representing the Antarctic Bottom Water in the model. The maximum values (about 18 Sv) of this stream function in CTL are found between 20°N–50°N and at depths around 800–1300 m. The simulated stream function compares very well with the observation-based estimation of 18.7 ± 2.1 Sv (Kanzow et al. 2010). In this study we define the AMOC strength index in the BCM2 as the maximum overturning stream function value between 20–50°N. The decadal time series of AMOC strength in CTL and the freshwater hosing experiments are shown in Fig. 3a. The AMOC in the FA, FE and FW simulations show a general weakening trend, with a total reduction of 14, 24 and 19 % in FA, FE and FW, respectively, compared to the mean of CTL during 1965–1999 (Table 1). In order to determine whether the weakening of the AMOC in each of the three experiments is forced significantly by the applied freshwater anomaly, or just within the natural variability, we analyzed 35-year length of segments (556) from CTL0 for their trends and mean values and compared them to the freshwater experiments (see Sect. 2.3 for details on the methodology). Some 35-year segments are shown in Fig. 3b. Here the trend is estimated by a first-order polynomial fit method, and the slope is used to evaluate the trend (units: Sv/35yr). All trend lines from a total of 565 CTL0 segments are plotted against those of the three freshwater-hosing experiments in

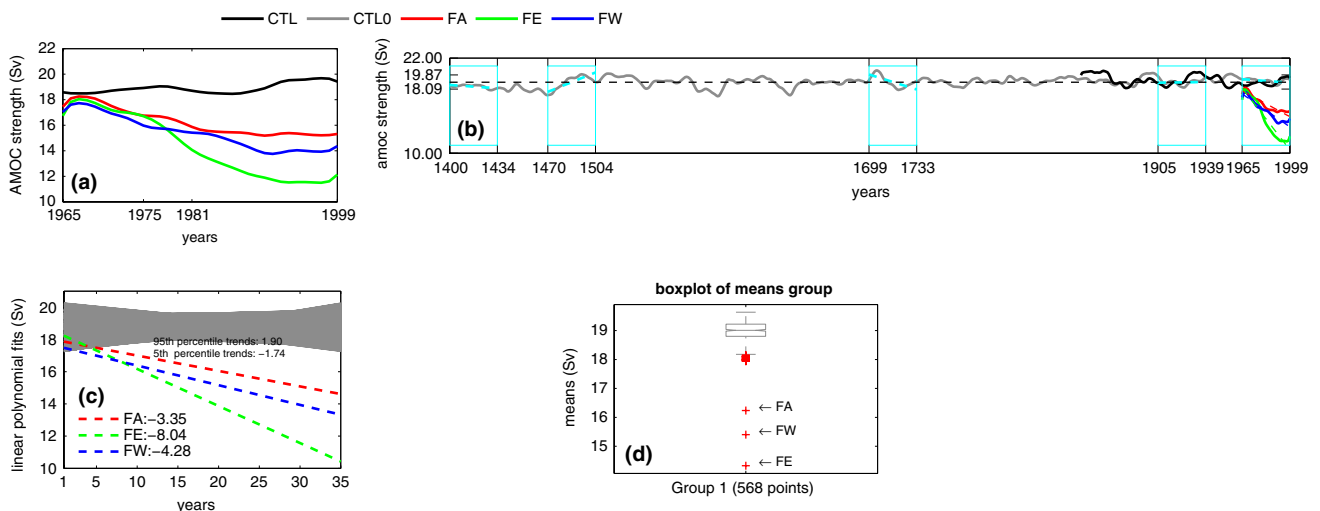


Fig. 3 a The evolution of decadal AMOC strength in CTL, FA, FE and FW (b) is same as (a) but for CTL0, FA, FE and FW. additionally some examples (by the rectangles) of 565 segments from CTL0 are shown (see detail in Sect. 2.3) c comparison between trend lines

(grey) of all the 565 segments against those of FA, FE and FW (d) boxplot of group consists of the mean values of all the 565 segments and of the FA, FE and FW. All the figures are based on annual values

Table 1 The annual averaged AMOC strength and volume transports across the 48°N section during whole integration, P1 and P2

Water mass	Exp.	Volume transport (1965–1999)	Volume transport (P1:1965–1980)	Volume transport (P2: 1981–1999)
AMOC strength	CTL	18.90 Sv	18.78 Sv	19.00 Sv
	FA	16.32	17.28	15.36
	FE	14.35 Sv	16.81 Sv	12.28 Sv
	FW	15.39 Sv	16.56 Sv	14.40 Sv
NADW (@layer 16–35)	CTL	18.46 Sv	18.52 Sv	18.41 Sv
	FA	14.54	15.52	13.56
	FE	10.26 Sv	14.28 Sv	6.89 Sv
	FW	12.38 Sv	14.27 Sv	10.78 Sv
CLSW (@layer 17)	CTL	5.1 Sv	5.5 Sv	4.7 Sv
	FA	1.9 Sv	2.7 Sv	1.1 Sv
	FE	2.6 Sv	4.2 Sv	1.2 Sv
	FW	1.8 Sv	2.6 Sv	1.04 Sv
ULSW (@layer 16)	CTL	7.4 Sv	7.0 Sv	7.8 Sv
	FA	6.5 Sv	6.8 Sv	6.2 Sv
	FE	3.4 Sv	5.1 Sv	1.8 Sv
	FW	5.3 Sv	6.2 Sv	4.4 Sv
Subpolar deep water	CTL	12.5 Sv	12.5 Sv	12.5 Sv
	FA	8.4 Sv	9.5 Sv	7.3 Sv
	FE	6.0 Sv	9.3 Sv	3.0 Sv
	FW	7.1 Sv	8.8 Sv	5.4 Sv
ODW (@layer 18–35)	CTL	5.6 Sv	5.5 Sv	5.7 Sv
	FA	5.3 Sv	5.5 Sv	5.12 Sv
	FE	5.32 Sv	5.6 Sv	5.2 Sv
	FW	5.31 Sv	5.3 Sv	5.1 Sv

Fig. 3c. From Fig. 3c, the 5th and 95th percentile of the trend ranges of the CTL0 are -1.74 and 1.90 (-1.68 and 2.01 in CTL by 115 35-year segments, not shown), while the trends are -3.35 in FA, -8.04 in FE and -4.28 in FW, respectively. Hence, the weakening trends in the three freshwater-hosing experiments are much stronger than the 5th percentile of the trend ranges of the CTL0, suggesting that it is unlikely that the weakening trend in each of the freshwater-hosing experiments is caused by nature variability in CTL0 or forced by the external forcing in CTL. Furthermore, the mean values of AMOC in the three freshwater-hosing experiments are all outliers compared to those values estimate from 556 35-year segments in CTL0 (and also to CTL, not shown) (Fig. 3d). The above results therefore strongly suggest that the weakening of AMOC in each freshwater-hosing experiment is indeed caused by the applied enhanced freshwater forcing.

It should be noted that the magnitudes in AMOC reduction among the three freshwater-hosing experiments are clearly different, with the AMOC in FE/FA being reduced the most/least (Table 1). It seems that the differences in AMOC strength among the three freshwater-hosing experiments are more evident after 1980 (Table 1; Fig. 3a). In

order to obtain a more precise decadal evolution of the differences among the three freshwater experiments, we calculated the low-pass filtered time series of the differences between FE and FW, FE and FA and FW and FA, respectively (Fig. 4a).

Firstly, we examine whether these differences between the three freshwater-hosing experiments are caused by the enhanced freshwater applied at the different coastal regions of Greenland, or they are just within the natural variability in CTL0. To do this, we computed the decadal anomalies of AMOC time series in CTL0 by subtracting the mean value over the 600-year integration (Fig. 4b). We then used the same method as described above to compare the differences from each of the three freshwater-hosing experiments, with those from CTL0 (Fig. 4c). The trend ranges of the CTL0 are -1.74 and 1.90 (units: Sv/35yr), while the trends are -3.84 for FE – FW, -4.69 for FE – FA and -0.93 for FW – FA (units: Sv/35yr), respectively. The differences between FE and FW and between FE and FA both show a declining trend over the 35-year integration period, likely caused by the different freshwater forcing. The trend of the difference between FW and FE, on the other hand, is within the natural variability of CTL0. A similar relationship is

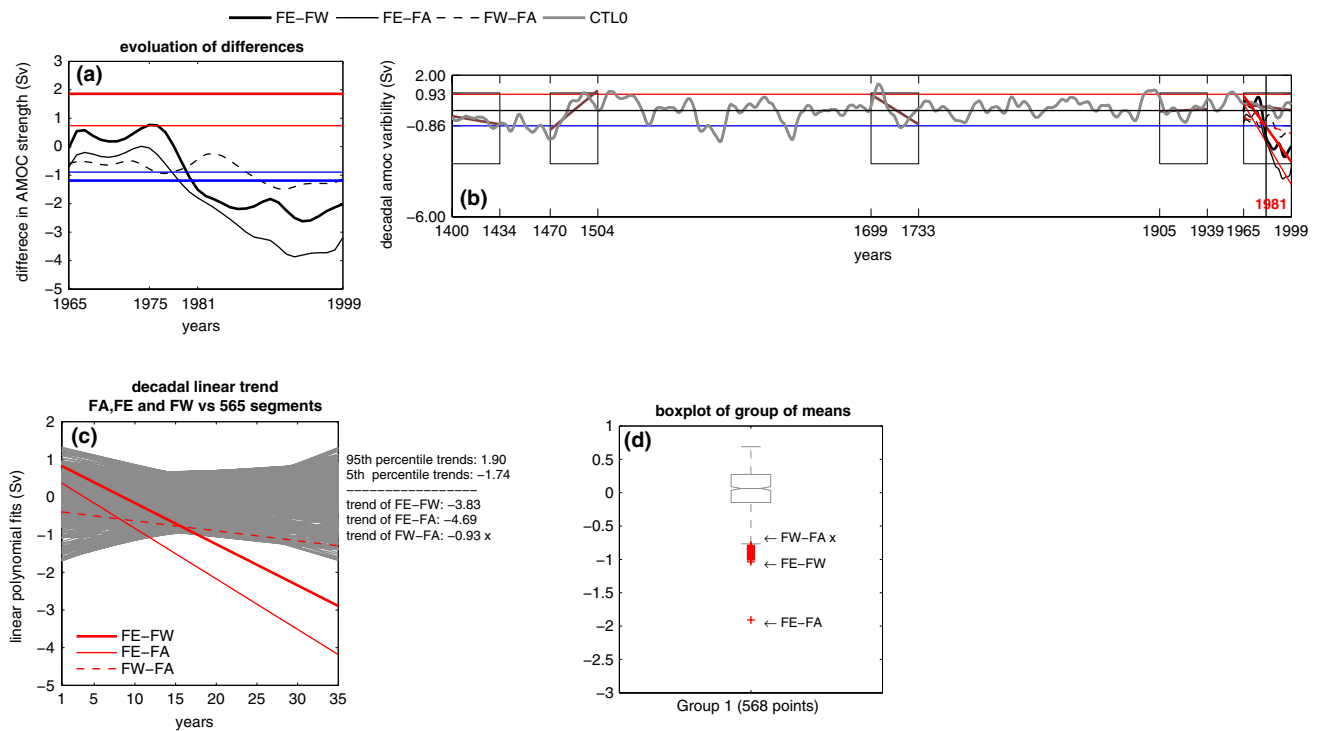


Fig. 4 **a** The evolution of decadal difference in AMOC strength of FE – FW, FE – FA and FW – FA. Additional the significance scopes based on performed Monte Carlo test (see details in Sect. 2.3) are also shown. The *bold (thin) red and blue straight line* denote the upper and lower confidence level for FE – FW (FE – FA), respectively. **b** The evolution of AMOC strength anomaly in CTL0 (related its climate mean over the 600 year of integration) and difference in AMOC strength of FE – FW, FE – FA and FW – FA. Additionally

some examples (by the *rectangles*) of 565 segments from CTL0 are shown (see detail in Sect. 2.3). The *red and blue straight lines* denote the 5th and 95th percentile of the decadal anomalies in CTL0, respectively. **c** comparison between the trend lines (*grey*) of all the 565 segments against those of FE – FW, FE – FA and FW – FA (**d**) a boxplot of group consists of the mean values of all the 565 segments and of FE – FW, FE – FA and FW – FA. All the figures are based on annual values

found for the mean values (Fig. 4d). Furthermore, we can see that the differences between FE and FW, between FE and FA are only becoming significant after about 1980 when comparing to natural variability induced from CTL0 (Fig. 4a, b) based on a Monte Carlo test (see Sect. 2.3 for details).

Our analysis indicates that the freshwater forcing applied along the eastern coast (FE) induce a weaker AMOC compared to the cases where the freshwater forcing is applied to the western coast (FW) or to the entire coast (FA) after about 20 years (hereafter refer to as P2). In the next sections, we will investigate the reason for the weakened AMOC in each of the freshwater-hosing experiments. In particular, we will focus on the differences in AMOC responses during P2 in the FE, FA and FW, respectively.

3.2 The mechanism for the weakening of AMOC in the freshwater experiments

The additional freshwater input along the different coastal regions of Greenland has a direct impact on the SSS in adjacent waters. In FA, a freshening occurs all around the

coast of Greenland during the early stage (P1 period), with strong negative salinity anomalies in the Labrador Sea (Fig. 5a). Later, during P2, the anomalies spread into the subpolar gyre as well as into the Nordic Seas (Fig. 5b). In FE (FW) the freshening can be seen in the western part of the open Nordic Seas (Labrador Sea) during P1 (Fig. 5c, e). In the P2 period, the negative salinity anomalies spread further into the subpolar gyre by the main ocean currents both in FE and FW as well as into the Nordic Seas (Fig. 5d, f).

For the SST, negative anomalies are found in the whole subpolar region and extend into the Nordic Seas in all the three freshwater-hosing experiments during P2 (Fig. 6a–c). They are likely the result of a reduced poleward heat transport due to the weakened AMOC in P1 (not shown). What should be emphasized is that the negative SST anomalies in the Labrador Sea in FE (about –1 to –2 °C on average) are weaker compared to those in FA (about –2 to –3 °C) and FW (about –4 to –5 °C). The importance of this difference will be addressed in Sect. 3.3.

The changes in the sea ice cover caused by additional freshwater input follow the SST anomalies in general

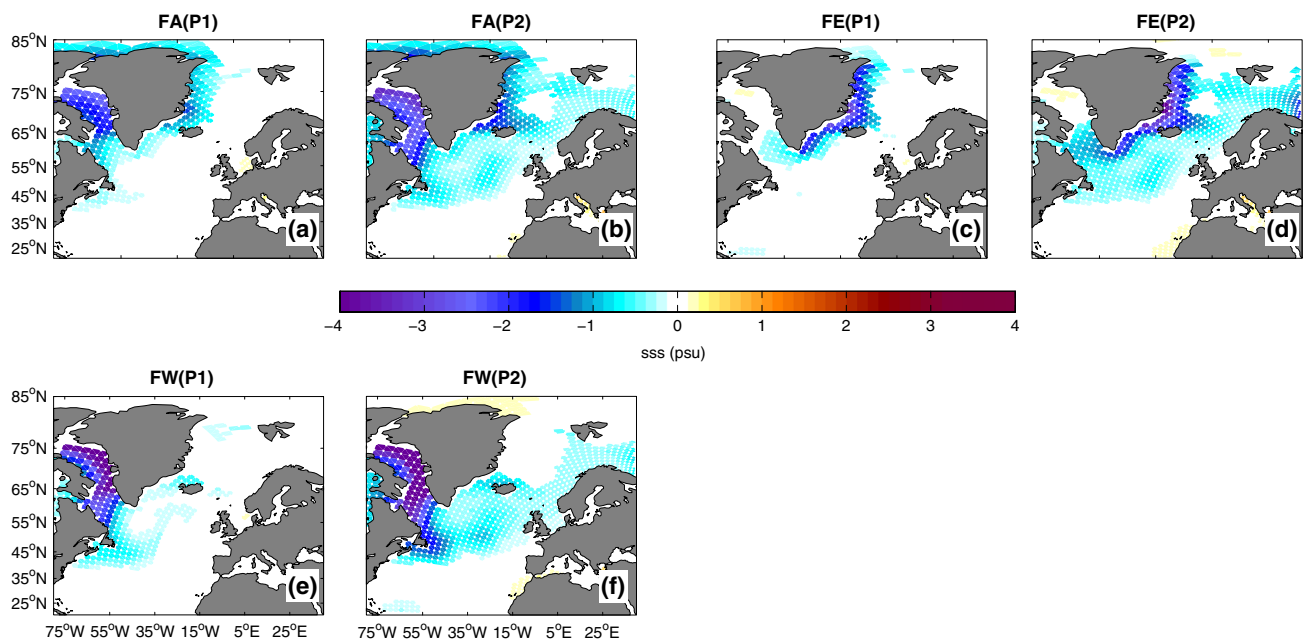


Fig. 5 The anomalies of SSS (psu) in FA (a for P1, b for P2), FE (c for P1, d for P2) FE, and FW (e for P1, f for P2). Only the anomalies that are identified as forced results (see details in Sect. 2.3) are

shown, and the confidence levels exceeding 95 % based on t test are denoted by the white dots in each map (dof = 36). All the figures are based on annual values

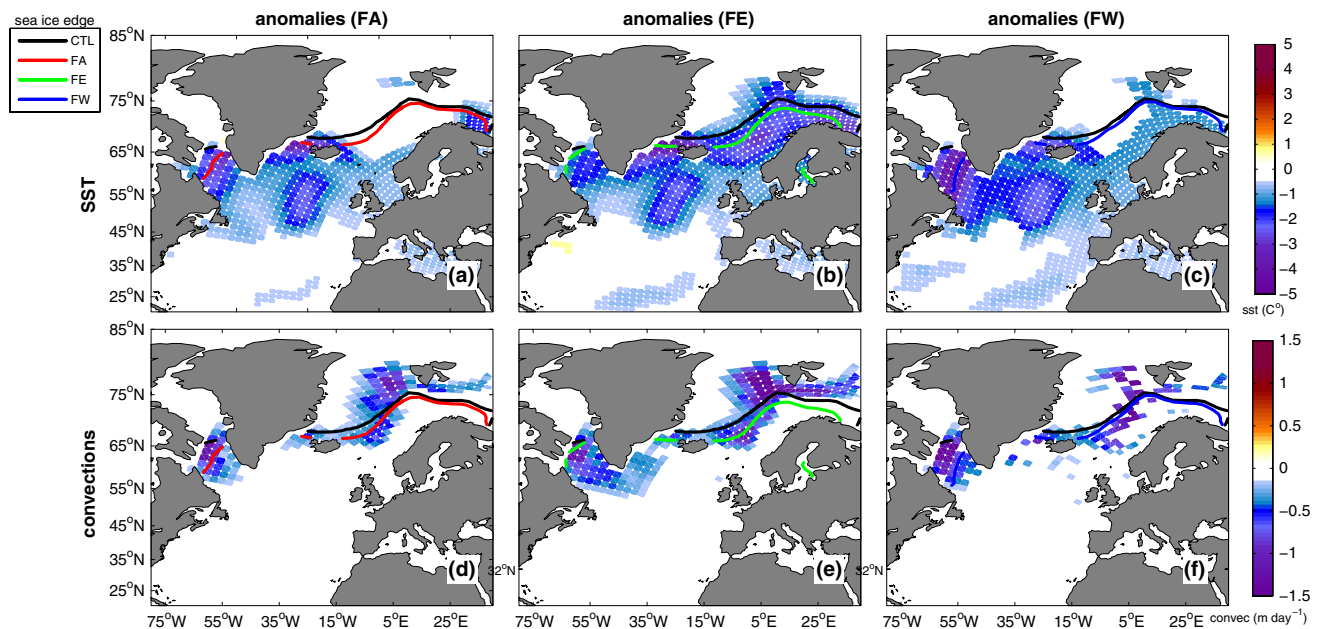


Fig. 6 As Fig. 5, but for anomalies in SST (a FA, b FE and c FW) and convection (d FA, e FE and f FW) in P2. SST anomalies are based on annual values, convection based on winter (Jan–Feb–Mar)

values. Additionally the annual-mean of sea ice covers (by sea ice concentration >15 %) in the CTL (black contour), FA (red contour) FE (green contour) and FW (blue contour) are shown in each map

(Fig. 6a–c). Compared to CTL, more sea ice can be seen in the Labrador Sea in FA and FW, while there are no noticeable changes of the sea ice cover in the Labrador Sea in FE. In contrast to the Labrador Sea, in the Greenland Sea

and Nordic Seas, a clear southward extension of the sea-ice cover can be seen in FE, but not in FA and FW.

In BCM2, the main winter convection occurs mainly in the Labrador Sea, the Irminger Sea and the Nordic

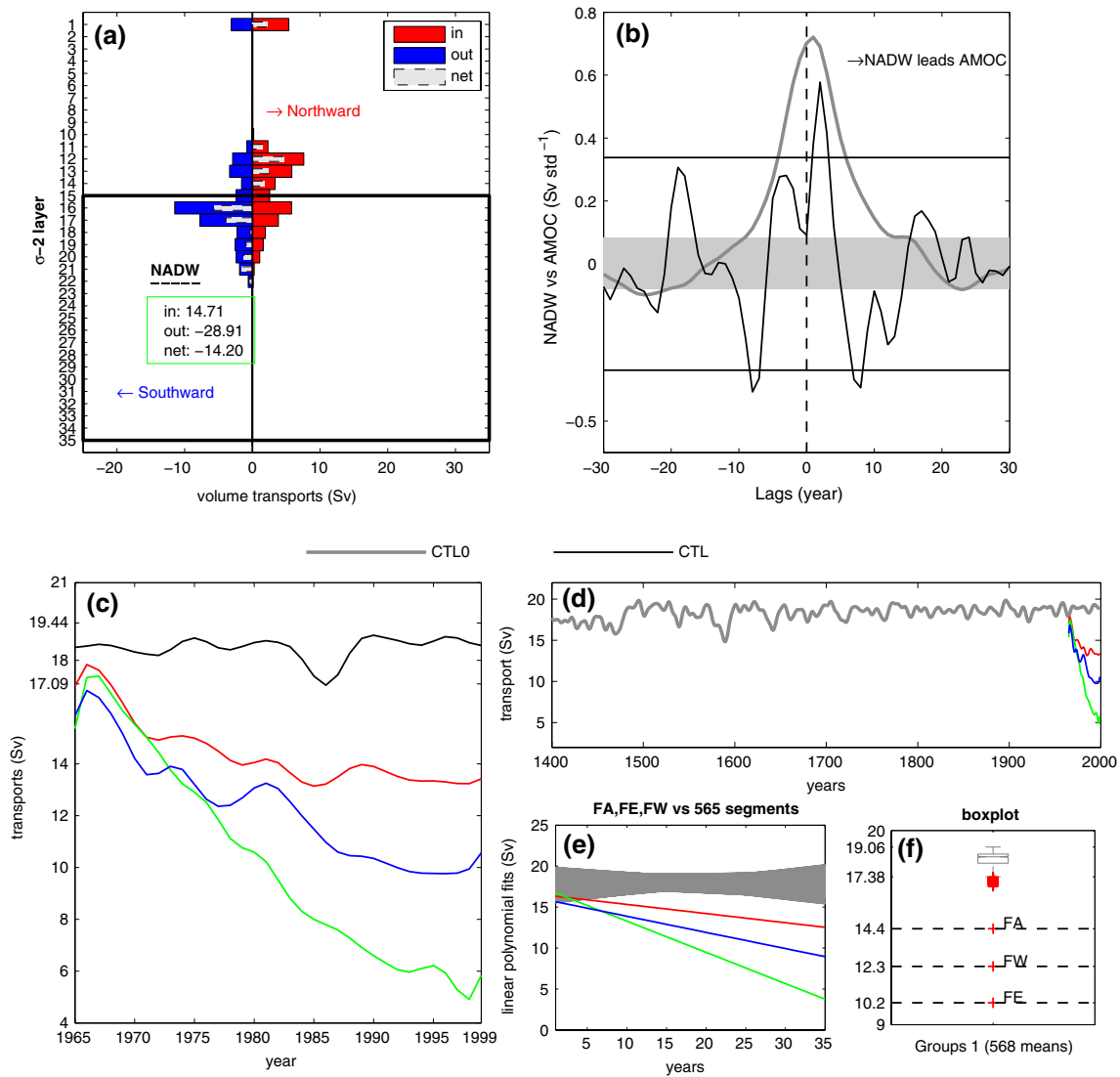


Fig. 7 a The CTL0-modeled climatic NADW transports (net deep southward transports occur at layer 16–35) through the latitudinal section of 48°N (b) the cross correlations between NADW transport and AMOC in CTL0 and CTL (c) the time series of the NADW transports through the latitudinal section of 48°N in CTL and in FA (red),

FE (green) and FW (blue) (d) same as (c) but for CTL0, FA, FE and FW. e, f trends examination on FA, FE and FW by CTL0 (see details in Sect. 2.3) (a) is averaged over the 150-year of integration. All the figures are based on annual values

Seas. The anomalies of surface buoyancy, caused by the additional freshwater input, have a direct influence on the convection in the Labrador Sea and the Irminger Sea. The negative SSS anomalies in the Labrador Sea lead to a reduction in convection in all freshwater-hosing experiments (Fig. 6d–f). Moreover, FE shows a further weakening of the convection in the southeastern Labrador Sea as well as in the Irminger Sea (hereafter we refer to this ocean region as seLab-sIrm region, see Fig. 9d for its position in the model). A general reduction in the convection can also be found in the central Nordic Seas in all freshwater-hosing experiments following the sea ice margin (Fig. 6d–f).

The generation of negative convection anomalies in the locations of the main deep-water formation are the main reason for explaining the weakening of AMOC in the three experiments. In particular, we find that the additional reduction of the convection in the seLab-sIrm region in FE is essential for the mechanism explaining the different sensitivity of the AMOC in FE compared to the other two experiments.

In order to address this in more detail, we show, as a first step, the CTL-simulated long-term mean (150-year) volume transport across the latitudinal section of 48°N (Fig. 7a). It follows that the net southward flow of intermediate-deep water masses occurs below σ_2 layer 16 (included) in the

model, with a total amount of about 18.5 Sv. This simulated NADW compares well with the observation-based estimate of 21 Sv (Pérez-Brunius et al. 2004). The lead-lag correlation between NADW and AMOC (Fig. 7b) shows that the NADW leads AMOC by 2 years, with correlations of 0.56 and 0.78 in CTL and CTL0, respectively. This indicates a dominant role of the NADW on the AMOC variability in BCM2, a feature that has been identified in previous studies (e.g., Otterå et al. 2009; Yu et al. 2009; Medhaug et al. 2012). Consistent with this, the NADW transports show common negative trends in all the three freshwater-hosing experiments (Fig. 7c). The significance tests indicate that the negative trends in NADW in each experiment are indeed caused by the added freshwater forcing, rather than internal variability alone (Fig. 7d–f).

The NADW comprises several water masses. It has been identified that four primary North Atlantic water masses make up NADW (e.g., Smethie et al. 2000). The least dense components of NADW are formed by deep ocean convection during winter, and are often referred to as the Classical Labrador Sea Water (CLSW) and the Upper Labrador Sea Water (ULSW, Pickart et al. 1996). The CLSW is mainly formed by deep convection in the central Labrador Sea, which can extend to depths as great as 2000 m. The ULSW is formed primarily by shallow convection in the southeastern part of the Labrador Sea (Langehaug et al. 2012) and in the southern Irminger Sea (Pickart et al. 2003a), or both (Pickart et al. 2003b). The densest components of the NADW are the overflowing deep water (ODW), which comprises the Denmark Strait overflow water and Iceland-Scotland overflow. In the BCM2, these water masses are generally well simulated (Medhaug et al. 2012). In the subpolar North Atlantic, the ULSW and CLSW are mainly represented at the σ_2 layer 16 ($\sigma_2 = 36.846$) and σ_2 layer 17 ($\sigma_2 = 36.946$), respectively, and the ODW are at σ_2 layers 19–35 ($\sigma_2 = 37.074$ to $\sigma_2 = 37.79$) (see Fig. 9 in Langehaug et al. 2012 and Fig. 9 in this study). In order to estimate the respective contributions of each water mass member to the weaker NADW in the freshwater-hosing experiments, the anomalies of CLSW and ULSW were calculated by means of their net southward volume transports through the 48°N in the North Atlantic. Following Zhu and Jungclauss (2008) and Lohmann et al. (2014), the overall changes in the water masses that are mainly formed in the subpolar region were evaluated by summing the transports changes of layer 16 and 17. For the contributions from the ODW that are mainly formed in the Nordic Seas, we calculated volume transports across the GSR into the subpolar North Atlantic. The results (Table 1) show that the southward transports of CLSW are reduced substantially during the P2, with reductions of 3.6 Sv in FA, 3.5 Sv in FE and 3.7 Sv in FW, respectively, compared to CTL. For the ULSW transports during the P2, they are reduced by 1.6 Sv

in FA, 6.0 Sv in FE and 3.4 Sv in FW, respectively, compared to CTL. The combined reduction in both CLSW and ULSW is 5.2 Sv in FA, less 9.5 Sv in FE and less 7.1 Sv in FW, respectively, compared to CTL. Among the three experiments, the subpolar deep water masses in FE are reduced by 2.4 Sv and 4.3 Sv in FW and FA, respectively, during the P2. The changes in ODW transports through the GSR are only minor compared to CTL during both P1 and P2.

To further confirm the reduction in deep water formation in the subpolar region, we show water mass anomalies using the isopycnic layer thickness (Fig. 8). It clearly shows a reduction of water masses in the subpolar region at the respective isopycnic layer in the three freshwater-hosing experiments compared to CTL. At the same time, more reductions of the ULSW in FE compared to FA and FW can be seen (Fig. 8b, e, h). The anomalies in layer thickness are consistent with the transport anomalies shown in Table 1.

The anomalously weak convection in the Labrador Sea and seLab-sIrm region is responsible for the reduced CLSW and ULSW formation, respectively. For the CLSW, the correlation between the convection in the Labrador Sea and CLSW has been reported in many observation-based and model studies (e.g., Otterå et al. 2009; Yu et al. 2009; Medhaug et al. 2012). Normally, when the NAO is in its positive phase, cold air is brought to the Labrador Sea, decreasing buoyancy and providing favourable conditions for the convective mixing. In this study, the surface buoyancy is increased by the reduced SSS in the Labrador Sea in each freshwater-hosing experiment compared to CTL. Subsequently the CLSW in each freshwater-hosing experiment shows a clear decline compared to CTL. The reduction in CLSW formation during P2 in each freshwater-hosing experiment is close to each other (Table 1; Fig. 8a, d, g).

For the ULSW, observations-based studies (Pickart et al. 1996) pointed out that this water mass is not a variety of CLSW, but rather a distinct water mass that is formed at a lower density than CLSW. Therefore, this water mass has also been referred to as Shallow Upper NADW in the literature (e.g., Rhein et al. 1995). The BCM2 captures this kind of water mass (Fig. 9a), which occurs mainly at the isopycnic layer 16 ($\sigma_2 = 36.846$) above CLSW. Early studies have suggested that the ULSW is formed by convection in the southern Labrador Sea, or partly formed by the convection in the Irminger Sea and southern rim of the Labrador Sea (Pickart et al. 2003b; Kieke et al. 2006; Langehaug et al. 2012). As shown in Fig. 9a, the maximum winter mixing layer depth (MXLD) in the seLab-sIrm region reaches 800–1500 m where the ULSW exists. The regression of the thickness of the layer 16 against the convection in the seLab-sIrm region (Fig. 9b) shows positive correlations in the

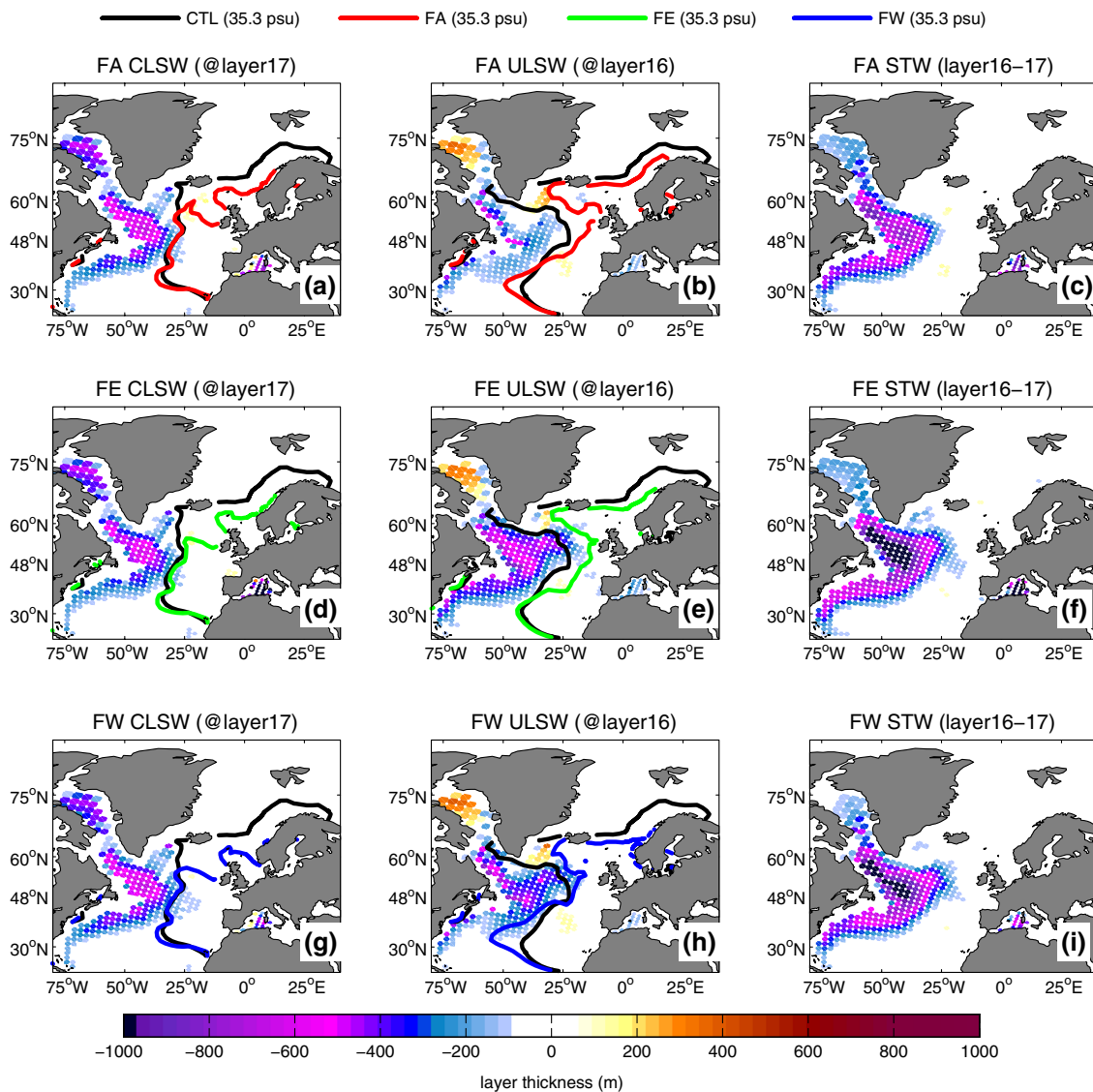


Fig. 8 The anomalies of layer thickness (m) of **a** CLSW (layer 17), **b** ULSW (layer 16) and **c** subpolar deep water (layer 16–17) in FA in P2; **d–f** are as **a–c** but for FE, and **g–h** are for FW. Additionally the contours of salinity 35.3 psu are shown to denote the main region of CLSW and ULSW (salinity < 35.3 psu) in each experiment (*black* for CTL, *red* for FA, *green* for FE and *blue* for FW). Only the anom-

lies that are identified as forced results (see details in Sect. 2.3) are shown, the white dots denote significance exceeding 95 % by *t* test confidence level (dof = 36). From *top* to *bottom* are for FA, FE and FW respectively, from *left* to *right* are for CLSW, ULSW and subpolar deep water. All the figures are based on annual values

area south of Greenland, with an extension into the Grand Banks, indicating a possible linkage between the formation of the ULSW and the convection in the seLab-sIrm region. We also note that the reduced convection is evident in the whole seLab-sIrm region in FE when compared to CTL, as opposed to the two other experiments where the convection anomalies are mainly located in the southeastern Labrador Sea (Fig. 6d–f). Hence, there is a common reduced ULSW formation in all freshwater-hosing experiments (Fig. 8b, e, h). However, a distinct difference exists in terms of the size of the reduction of the water masses. During the P2, ULSW

formation in FE is 4.4 Sv lower than that in FA (1.8 vs. 6.2), and is 2.6 Sv lower than that in FW (1.8 vs. 4.4). The CLSW formation in FE is 1.7 Sv lower than that in FA, but 0.2 Sv higher than that in FW (Table 1; Fig. 8). The latter is associated with the direct freshwater forcing close to the Labrador Sea in FW. Thus, our results clearly indicate that the reduced ULSW formation is the major contributor to the stronger weakening of the NADW in FE compared to the other two freshwater hosing experiments.

The reduced convection in the central Nordic Seas seems to have limited effect on the ODW transports through GSR

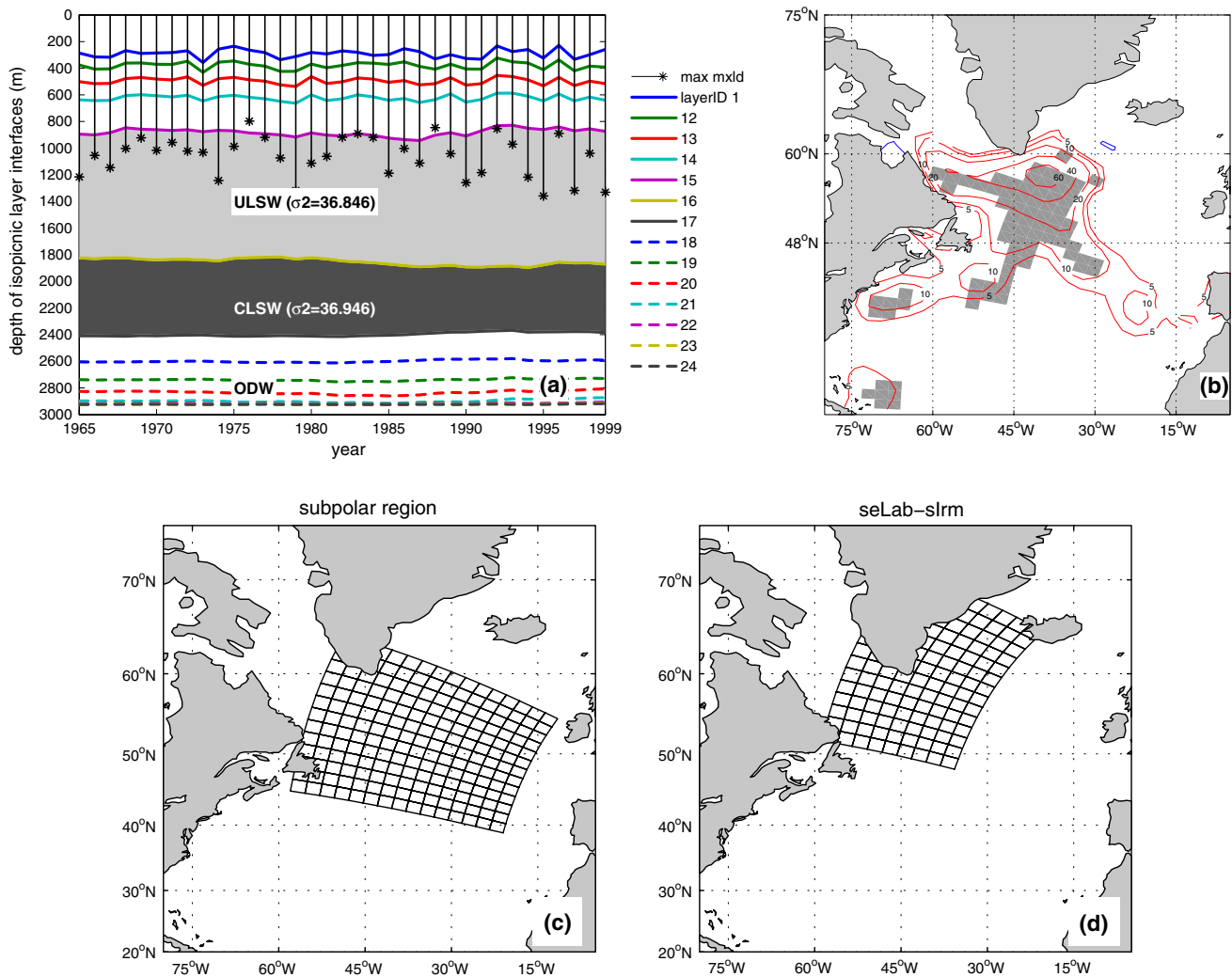


Fig. 9 **a** The time series for the yearly depth of the layer interfaces (m, colour lines) in the subpolar region and maximum depth that the winter mixing in the seLab-sIrm region reaches (m, black line-dots); **b** lagged (=1 year) correlations (m std⁻¹) between the previous winter convection in the seLab-sIrm region and followed year mean thickness of layer 16 (ULSW) in CTL. Correlations are computed

based on the standardized (std) value of convection due to value order and units of convection (m day⁻¹) is different from the layer depth (m), and significance exceeding 95 % confidence level are shaded; **c** is the grids position used to calculate the layer thickness shown in **(a)**; **d** is the grids position used to calculate the regression in **(b)**. **a**, **b** are based on 150-year CTL results

into the subpolar gyre (Table 1). This is likely due to the fact that some of the dense water masses formed by the convection in the Nordic Seas will end up below the sill depth of the GSR (Hansen et al. 2010; Langehaug et al. 2012). In this study, our results show only a minor contribution of the ODW to the anomalies and differences in NADW formation among the freshwater-hosing experiments. Medhaug et al. (2012) pointed out that in BCM2 the deep convective mixing is not necessarily an ideal measure of the total water mass transformation in the Nordic Seas. They suggested that the water mass exchange across the GSR is associated with the so-called Scandinavia pattern. This pattern dominates the poleward heat transport into the Nordic Seas. During a negative phase of the Scandinavian Pattern, there

are stronger than normal northerly winds blowing over the Nordic Seas (see Fig. 13 in Medhaug et al. 2012). This sets up an increased Ekman transport towards Greenland and the sea ice edge, with associated elevated sea surface height in the western part of the Nordic Seas and lower sea surface height in the eastern part. The associated pressure gradient changes give rise to increased barotropic circulation in the Nordic Seas that ultimately is driving more PHT into the Nordic Seas (Medhaug et al. 2012).

Finally, significantly reduced southward transports of NADW across the 48°N section in all the freshwater-hosing experiments can be seen after around 1980 (Fig. 7). During P2 the reduction in NADW transport amounts to about 4.8 Sv in FA, 11.5 Sv in FE and 7.6 Sv in FW, respectively,

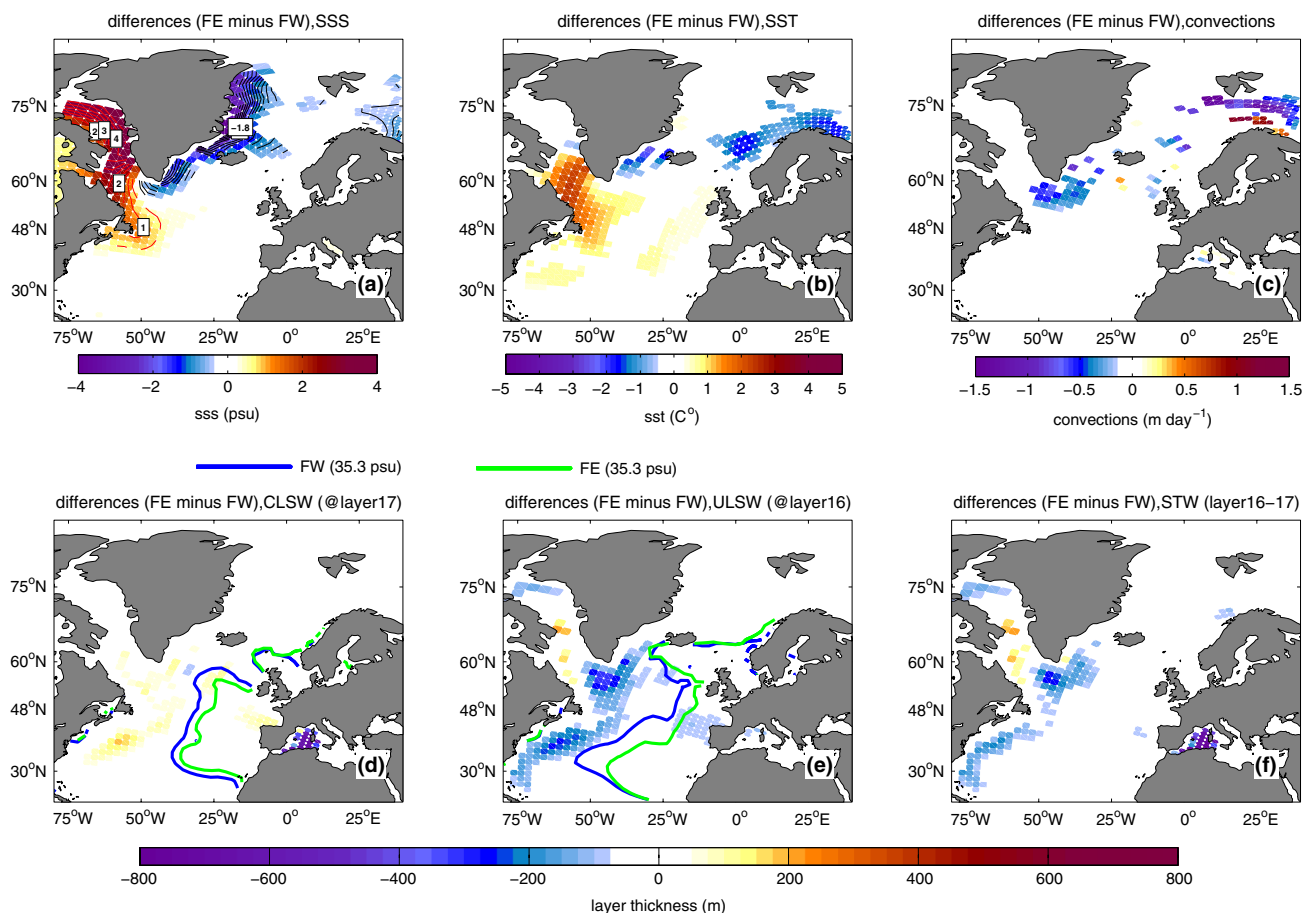


Fig. 10 The differences between FE and FW in P2. **a** SSS, **b** SST, **c** winter convection **d** CLSW, **e** ULSW, **f** subpolar deep water. Only the differences that are identified as forced results (see details in

Sect. 2.3) are shown, and the confidence levels exceeding 95 % based on *t* test are denoted by the *white dots* in each map (dof = 36). All the figures are based on annual values except (c) winter convection

when compared to CTL. Following the substantial reduction in NADW transports across the 48°N, the AMOC in each freshwater-hosing experiment is weakened, with FE showing the strongest decline. The presented analyses therefore point to a decisive role of the convective activities in the seLab-sIrm region and the related formation of the ULSW in leading to the strong weakening of AMOC in FE.

3.3 FE compared against the FW and FA

In Sect. 3.2, the key role of the convective activities in the seLab-sIrm region in causing the differences between the FE and the other experiments was found. In this section we focus on the mechanism and the cause for the reduced convection in the seLab-sIrm region in FE compared to FA and FW. The differences in SSS between FE and FW show a dipole pattern with relative fresher water masses along the eastern coast of Greenland and relative saline water masses in the Labrador Sea (Fig. 10). Based on such differences in SSS, one might expect stronger winter convective

activities in the Labrador Sea and more deep water mass formation in FE compared to FW. However, no significant difference in convection in the Labrador Sea can be seen between these two experiments (Fig. 10c). There are several reasons for this. Firstly, as mentioned previously (see Sect. 3.1), relatively warmer waters are found in the Labrador Sea in FE compared to FW (Fig. 10b). This is partly due to the reduced heat loss from the Labrador Sea to the atmosphere (Fig. 11b). Secondly, the differences in sea level pressure (SLP) between FE and FW (Fig. 11c) show positive anomalies over Greenland and the Nordic Seas, but negative anomalies over the Labrador Sea extending into the subpolar gyre. Associated with this negative NAO-like pattern, there are anti-cyclonic winds developing along the southern rim of Greenland and northerly winds through the GSR. Such a wind-SLP difference is set up already during the first 1–2 years (not shown), and persists for most years during the whole integration period. The southerly winds over the Labrador Sea in FE compared FW have two main consequences: (1) they bring more warm air mass into the

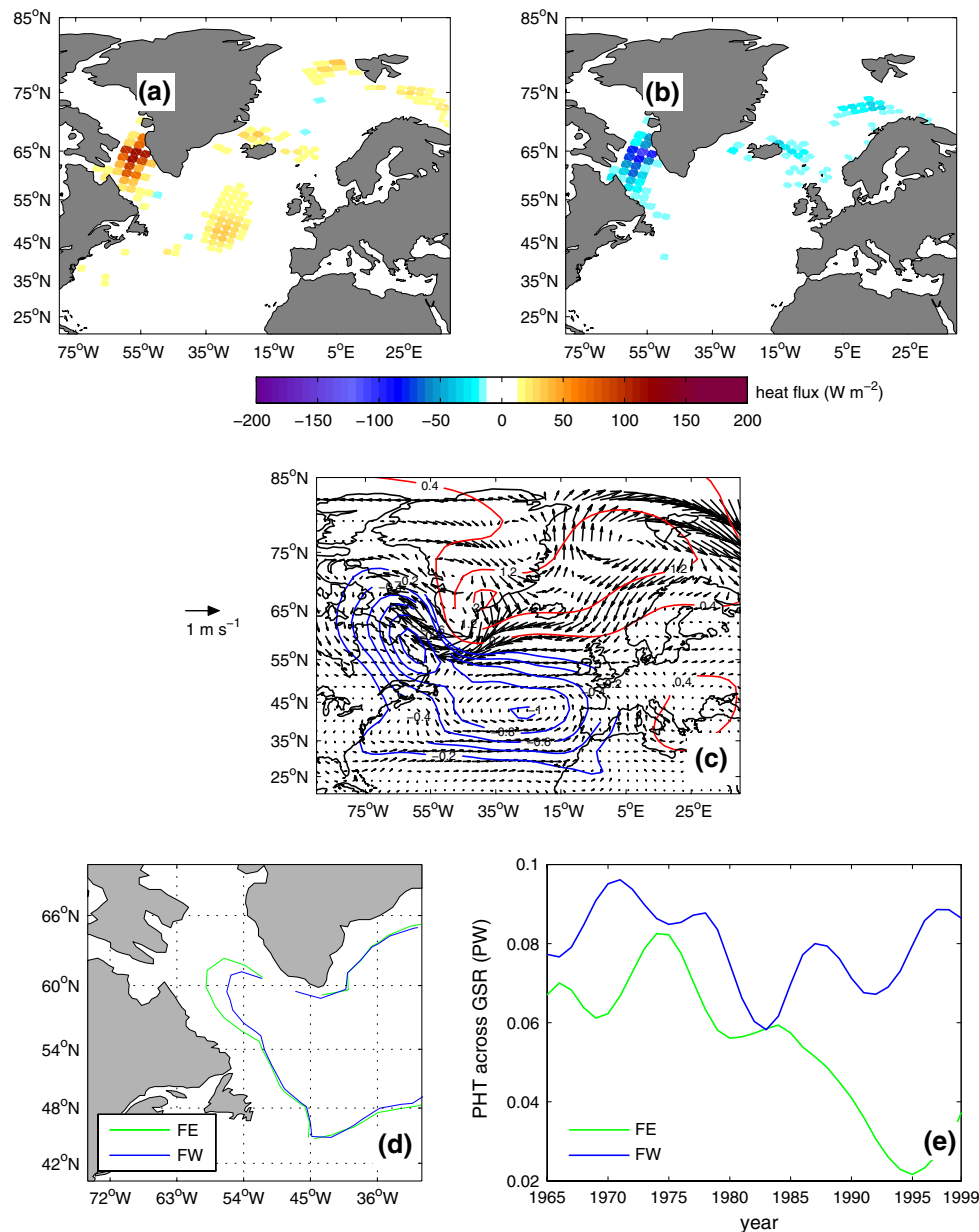


Fig. 11 **a** anomalies of winter heat flux (Jan–Feb–Mar) in the FE; **b** difference of heat flux between FE and FW (FE – FW) in P2; **c** the significant differences of surface winds (vectors) and sea level pressure (contours) in P2; **d** the subpolar gyre edge (denoted by the -5 contour of surface barotropic stream function) in the FE and FW in P2 and **e** the evolution of PHT across the GSR in the FE and FW.

c, d, the negative values denote the reduced heat loss from ocean to atmosphere. Only the anomalies and differences that are identified as forced results (see details in Sect. 2.3) are shown in (a)–(c), and the confidence levels exceeding 95 % based on t test (dof = 36) are denoted by the *white dots*. All the figures are based on annual values except (a)

Labrador Sea and cause a westward shift of the subpolar gyre in FE compared to FW (Fig. 11d), and (2) they lead to a reduced sea ice cover and associated surface albedo in the Labrador Sea in FE compared to FW (Fig. 6e, f). The latter again provides a positive feedback to the reduced ocean heat loss here (Fig. 11b). In addition, the westward shift of the subpolar gyre in FE compared to FW (Fig. 11d) can drive more warm Atlantic water with the North Atlantic

Currents into the Labrador Sea. Finally, the combination of these oceanic and atmospheric processes result in a relative warming in the Labrador Sea in FE compared to FW, as shown by Fig. 10b. On the other hand, the anomalous northerly winds through the GSR in FE compared to FW reduce PHT into the Nordic Seas (Fig. 11e), resulting the relative cold sea water in the Nordic Seas in FE compared to FW.

Therefore, although the convection in the Labrador Sea might intuitively be assumed to be stronger in FE compared to FW, the concurrent warming in the Labrador Sea in FE compared to FW counteracts the freshwater forcing impact on the convection in the Labrador Sea. Consequently, there are no significant differences in the convection in the Labrador Sea between FE and FW during the P2. Meanwhile, the additional freshwater forcing from the eastern coast of the Greenland in FE reduces the convection in the seLab-sIrm region. Additionally the anticyclone-like winds along the southeast rim of Greenland in FE compared to FW (Fig. 11d) are actually representing a negative Greenland tip jet pattern (Pickart et al. 2003a, b; Våge et al. 2008); it can weaken the convection in the seLab-sIrm region, as indicated by Pickart et al. (2003a). Finally, the weaker convection in the seLab-sIrm region in FE leads to much less formation of ULSW and then less subpolar deep water masses in FE compared to FW (Fig. 10f), although there is marginally more CLSW water masses in FE compared to FW (Fig. 10d).

The key processes described above can also be seen in the comparison between FE and FA (Fig. 12). This includes a relatively warmer Labrador Sea (Fig. 12b), weaker convection in the seLab-sIrm region (Fig. 12c), more reduced heat loss from the Labrador Sea to the atmosphere (Fig. 12g) and the occurrence of a negative Greenland tip jet pattern (Fig. 12h). In fact, the differences between FE and FA are even more evident compared to the difference between FE and FW. Consequently the ULSW and subpolar deep water formations are more reduced in FE compared to FA (Fig. 12e, f). The end result is a much weaker AMOC in FE compared to FA.

The above results highlight an important role of the convective activities in the seLab-sIrm region, and the related formation of the CLSW, for the sensitivity of AMOC to a large freshwater anomaly along the eastern coast of Greenland.

4 Discussion

We have described the responses of the simulated AMOC in BCM2 to a large freshwater anomaly of 0.1 Sv released around the entire Greenland coast, as well as the eastern and western coasts of Greenland. Here the 0.1 Sv of the freshwater is used as an accumulated amount of freshwater input. The total GrIS melting contribution over 2081–2100 is projected to about 0.12 m, with a likely high range of 0.21 m under the RCP8.5 scenario (Church et al. 2013). Accordingly the melting rate is about 6 mm per year, with an upper limit of 10.5 mm per year over 20 years, which is about 0.12 Sv freshwater inputs from GrIS melting during the period 2081–2100. Furthermore, the rate of GrIS

melting reported by the IPCC AR5 models could be conservative (Blaschek et al. 2015). If the observed recent increasing in GrIS melting rates (Bamber et al. 2012; Shepherd et al. 2012) continue, the GrIS melting rates in the future are likely to exceed previous projections. This is also taken into account in the choice of 0.1 Sv for the freshwater forcing in our experiments. Regardless of this, the presented simulations in this study should be view as high-end experiments only.

It should also be noted that the present study is based on only one climate model. An important limitation of this model is the coarse resolution of the ocean model. For instance, the limited grid resolution in the Nordic Seas could reduce the emergence of relative warm subsurface Atlantic sea water, resulting in anomalous cooling in the Nordic Seas. It is different from the anomalous warming in the Nordic Seas found in some other freshwater-hosing experiments (i.e., Stouffer et al. 2006; Saenko et al. 2007; Kleinen et al. 2009). In this study the cooling in the Nordic Seas is a general response of all the three experiments, suggesting it is not related to the locations of the freshwater released. Meanwhile we find that the changes in the ODW from the Nordic Seas into subpolar gyre through the GSR have limited contributions to the anomalies and differences in AMOC among our freshwater experiments. It is therefore uncertain to which degree the warming in the Nordic Seas found in some higher-resolution ocean models could lead to different responses in the deep water masses formed in the Nordic Seas in each of the freshwater-hosing experiment. Such uncertainty needs to be addressed by further multi-model simulations. Also, there are only 2–3 grid points that allow for the representation of the dynamics of the Denmark Strait, which could cause excessive mixing of the additional freshwater into the Denmark Strait and Nordic Seas. On the contrary, multi-model comparison (Swingedouw et al. 2013) found that the enhanced freshwater can escape from western Greenland into the subtropics in all models except BCM2 (see their Fig. 2). However, if such a freshwater leakage would have also taken place in BCM2, the freshwater leakage would make the added freshwater released along the western coast of Greenland in FW and FA escape into the subtropics rather than spread into the Irminger Sea and Denmark Strait. In this case, the weaker convection found in FE could be more evident compared to FW and FA because of the fact that in FE the added freshwater is directly released into the Irminger Sea and Denmark Strait. This would result in a further reduction in formation of ULSW masses and subsequently a weaker AMOC in FE compared to FW and FA (see Sect. 3.3).

Moreover, similar results to the present study were obtained in some other freshwater-hosing experiments. Smith and Gregory (2009) also documented a wide range of AMOC responses depending on the region of freshwater release. We

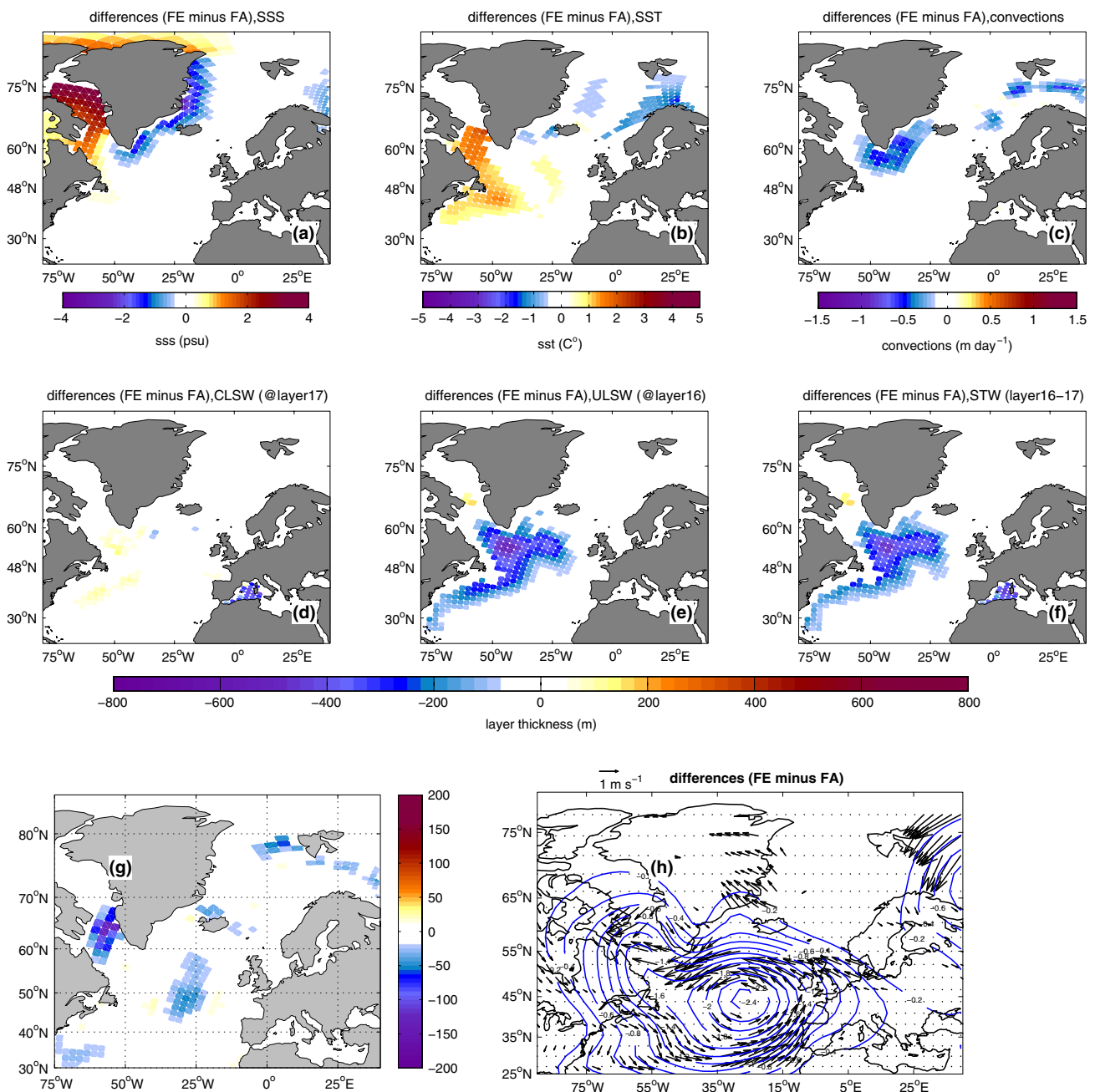


Fig. 12 Comparison between FE and FA. **a–f** is as Fig. 10a–f but for FE – FA in P2. **g–h** is as for Fig. 11b–c but for FE – FA in P2

note that in their Fig. 3, the strength of the AMOC in their 65 W experiment, in which the freshwater was added into the east Greenland coast, is weaker than that in their LAB experiment, where the freshwater was applied to the Labrador Seas. In the study of Saenko et al. (2007), a freshwater anomaly of 1 Sv was released along the southwestern coast of Greenland. Their result showed significant increased surface temperatures in the Labrador Sea region and easterly winds over the southern Irminger Sea in their experiments as compared to their unforced run. These anomalies are quite similar

to the relatively warm Labrador Sea water and the negative Greenland Jet-like pattern found in FE compared to FW and FA. Because of the rather large anomaly of freshwater input (1 Sv) that was used in their studies, the anomalies are evident even when compared directly to their control run. However, we note that the horizontal resolution of the ocean part in their climate model is $1.41^\circ \times 0.94^\circ$, which is much finer than the model used in this study. These similar results indicate that our results and the proposed mechanism could be robust although based on the coarse-resolution ocean model.

Some other freshwater-hosing experiments (i.e. Junglaus et al. 2006; Fichefet et al. 2007) have suggested that only under the extreme scenario of a future warming state, can the GrIS melting (i.e. the 0.1 Sv) all round Greenland induce a noticeable AMOC weakening. In this study we suggest that the AMOC can be more sensitive to enhanced freshwater forcing along the eastern side of Greenland as opposed to a case where the freshwater discharge is synchronous on both the eastern and western coasts. Thus, a stronger sensitivity of AMOC to the GrIS melting from eastern side of Greenland may not be excluded in the future given a sufficiently warm climate. In order to properly address this issue, further research is needed, preferably by using much longer freshwater-hosing experiments. Because of the short integration period in this study, we cannot provide a long-term perspective of the potential AMOC responses to GrIS melting. Thus, to what extent the AMOC will continue to be weakened by the proposed mechanism in this study, or whether it will recover by feedbacks from other potential processes from ocean or atmosphere, remains uncertain. Much longer freshwater-hosing experiments, with multi-model simulations, are therefore needed to address this issue.

5 Summary and conclusions remarks

In this study the sensitivity of AMOC to GrIS melting along the entire, east and west of Greenland under present-day climate state is investigated. Our main results are: (1) a general weakened AMOC is obtained in all of the freshwater-hosing experiments; (2) the simulated AMOC is more sensitive to the freshwater released along the eastern coast of Greenland compared to the other two experiments. The mechanism can be summarized as follows:

- (1) The added freshwater input can penetrate into the Labrador Sea regardless of where it is released through advection by Greenland currents. This reduces the convection in the Labrador Sea and associated formation of Labrador Sea water masses, and lead to a general weakening of AMOC in all of the freshwater experiments.
- (2) The most weakened AMOC is found in FE compared to the other experiments. This is mainly due to less formation of ULSW in FE. Firstly, the warming in the Labrador Sea in the FE compared to the other two experiments give a negative feedback to the CLSW formation in FE, although the SSS in the Labrador Sea is higher in the FE compared to the other two experiments. Subsequently the differences in CLSW formation in the FE compared to the other two experiments are not very evident. At the same time the additional

freshwater input along the eastern coast of Greenland, together with a negative Greenland tip jet-like wind pattern response, leads to weaker convection in the southeastern rim of Greenland and the southern Irminger Sea in FE compared to the other two experiments. This induces substantially less ULSW formation, which contributes to less NADW being formed in FE compared to the other two experiments. The end result is a weaker AMOC in FE compared to the other two experiments.

Admittedly the results presented here are based on only one coupled model. Further investigations based on multi-models results are clearly warranted. Nevertheless our mechanism could provide a way to estimate the responses of AMOC to the ongoing increased GrIS melting before such multi model results are available. An important aspect here will then be to not only consider the AMOC sensitivity to the GrIS melting all around Greenland, but also to take into account the potential consequences of a more regional freshwater release, such as along the eastern Greenland.

Acknowledgments The simulations and analysis in this study were supported by the European Union's Seventh Framework Program (THOR; Grant No. 212643), the National Basic Research Program of China (Grant No. 2009CB421401) and the Strategic Priority Research Program (Grant No. XDA05110203) of the Chinese Academy of Sciences, respectively. This study is also a contribution to the Centre for Climate Dynamics at the Bjerknes Centre, Bergen, Norway. We thank three anonymous reviewers for their very useful comments that improved the manuscript.

References

- Bakker P, Van Meerbeek CJ, Renssen H (2012) Sensitivity of the north atlantic climate to greenland ice sheet melting during the last interglacial. *Clim Past* 8:995–1009
- Bamber J, Broeke MVD, Ettema J, Lenaerts J, Rignot E (2012) Recent large increases in freshwater fluxes from Greenland into the north Atlantic. *Geophys Res Lett* 39(19):L19–L501. doi:10.1029/2012GL052552
- Blaschek M, Bakker P, Renssen H (2015) The influence of Greenland ice sheet melting on the Atlantic meridional overturning circulation during past and future warm periods: a model study. *Clim Dyn* 44:2137–2157
- Bleck R, Rooth C, Hu D, Smith LT (1992) Salinity-driven thermocline transient in a wind- and thermohaline-forced isopycnic coordinate model of the North Atlantic. *J Phys Oceanogr* 22:1485–1505
- Boyle EA, Keigwin LD (1987) North Atlantic thermohaline circulation during the past 20000 years linked to high latitude surface temperature. *Nature* 330:35–40
- Broecker WS (1991) The great ocean conveyor. *Oceanography* 4:79–89
- Bryan F (1986) High-latitude salinity effects and interhemispheric thermohaline circulations. *Nature* 323:301–304
- Chen JL, Wilson CR, Tapley BD (2006) Satellite gravity measurements confirm accelerated melting of Greenland ice sheet. *Science* 313:1958–1960

- Christoffersen P, Mugford RI, Heywood KJ et al (2011) Warming waters in an East Greenland fjord prior to glacier retreat: mechanisms and connection to large-scale atmospheric conditions. *Cryosphere* 5:701–714. doi:[10.5194/tc-5-701-2011](https://doi.org/10.5194/tc-5-701-2011)
- Church JA, Clark PU, Cazenave A, et al (2013) Sea level change. In: Stocker TF, Qin D, Plattner G-K, et al (eds) *Climate change 2013: the physical science basis. Contribution of working group I to the fifth assessment report of the intergovernmental panel on climate change*. Cambridge University Press, Cambridge
- Déqué M, Drevet C, Braun A, Cariolle D (1994) The ARPEGE/IFS atmosphere model: a contribution to the French community climate modelling. *Clim Dyn* 10:249–266
- Dickson B, Yashayaev I, Meincke J, Turrell B, Dye S, Holfort J (2002) Rapid freshening of the deep North Atlantic Ocean over the past four decades. *Nature* 416:832–837
- Fettweis X, Tedesco M, van den Broeke M, Ettema J (2011) Melting trends over the Greenland ice sheet (1958–2009) from spaceborne microwave data and regional climate models. *Cryosphere* 5:359–375. doi:[10.5194/tc-5-359-2011](https://doi.org/10.5194/tc-5-359-2011)
- Fichefet T, Driesschaert E, Goosse H, et al. (2007) Modelling the influence of Greenland ice sheet melting on the Atlantic meridional overturning circulation during the next millennia. *Geophys Res Abs* 9: 02554. SRef-ID: 1607-7962/gra/EGU2007-A-02554
- Franzke C (2011) Nonlinear trends, long-range dependence, and climate noise properties of surface temperature. *J Clim* 25:4172–4183
- Furevik T, Bentsen M, Drange H et al (2003) Description and evaluation of the Bergen climate model: ARPEGE coupled with MICOM. *Clim Dyn* 21:27–51
- Gao Y, Drange H, Bentsen M (2003) Effects of diapycnal and isopycnal mixing on the ventilation of CFCs in the North Atlantic in an isopycnal coordinate OGCM. *Tellus* 55B:837–854
- Geleyn J-F (1988) Interpolation of wind, temperature and humidity values from model levels to the height of measurement. *Tellus (A)* 40:347–351
- Giles KA, Laxon SW, Ridout AL, Wingham DJ, Bacon S (2012) Western Arctic Ocean freshwater storage increased by wind driven spin-up of the Beaufort Gyre. *Nat Geosci* 5:194–197. doi:[10.1038/ngeo1379](https://doi.org/10.1038/ngeo1379)
- Hansen B, Hátún H, Kristiansen R, Olsen SM, Østerhus S (2010) Stability and forcing of the Iceland-Faroe inflow of water, heat and salt to the Arctic. *Ocean Sci* 6:1013–1026. doi:[10.5194/os-6-1013-2010](https://doi.org/10.5194/os-6-1013-2010)
- Jungclauss JH, Haak H, Esch M et al (2006) Will Greenland melting halt the thermohaline circulation? *Geophys Res Lett* 33:L17708
- Kanzow T, Cunningham SA, Johns WE et al (2010) Seasonal variability of the Atlantic meridional overturning circulation at 26.5°N. *J Clim* 23:5678–5698
- Kieke D, Rhein M, Stramma L et al (2006) Changes in the CFC inventories and formation rates of upper Labrador Sea Water, 1997–2001. *J Phys Oceanogr* 36:64–86
- Kleinen T, Osborn TJ, Briffa KR (2009) Sensitivity of climate responses to variations in freshwater hosing location. *Ocean Dyn* 59:509–521. doi:[10.1007/s10236-009-0189-2](https://doi.org/10.1007/s10236-009-0189-2)
- Langehaug HR, Medhaug I, Eldevik T, Otterå OH (2012) Arctic/Atlantic exchanges via the subpolar gyre. *J Clim* 25:2421–2439. doi:[10.1175/JCLI-D-11-00085.1](https://doi.org/10.1175/JCLI-D-11-00085.1)
- Lohmann K, Jungclauss J, Matei D et al (2014) The role of subpolar deep water formation and Nordic Seas overflows in simulated multidecadal variability of the Atlantic Meridional overturning circulation. *Ocean Sci* 10:227–241
- Louis J (1979) A parametric model of vertical eddy fluxes in the atmosphere. *Bound Lay Meteorol* 17(187):202
- Manabe S, Stouffer RJ (1995) Simulation of abrupt climate change induced by freshwater input to the North Atlantic Ocean. *Nature* 378:165–167
- Manabe S, Stouffer RJ (1997) Coupled ocean-atmosphere model response to freshwater input: comparison to Younger Dryas event. *Paleo-oceanography* 12:321–336
- Manabe S, Stouffer RJ (1999) The role of thermohaline circulation in climate. *Tellus* 51:91–109
- Marzeion B, Levermann A (2009) Stratification-dependent mixing may increase sensitivity of a wind-driven Atlantic overturning to surface freshwater flux. *Geophys Res Lett* 36:L20602. doi:[10.1029/2009GL039947](https://doi.org/10.1029/2009GL039947)
- Marzeion B, Levermann A, Mignot J (2007) The role of stratification-dependent mixing for the stability of the Atlantic overturning in a global climate model. *J Phys Oceanogr* 37:2672–2681
- McDougall TJ, Dewar WK (1998) Vertical mixing and cabbeling in layered models. *J Phys Oceanogr* 28:1458–1480
- Medhaug I, Langehaug HR, Eldevik T, Furevik T, Bentsen M (2012) Mechanism for decadal scale variability in a simulated Atlantic meridional overturning circulation. *Clim Dyn* 39:77–93
- Mikolajewicz U, Vizcaino M, Jungclauss J et al (2007) Effect of ice sheet interactions in anthropogenic climate change simulation. *Geophys Res Lett* 34:L18706. doi:[10.1029/2007GL031173](https://doi.org/10.1029/2007GL031173)
- Mohammad R, Nilsson J (2004) The role of diapycnal mixing for the equilibrium response of the thermohaline circulation. *Ocean Dyn* 54:54–65
- Nilsson J, Broström G, Walin G (2003) The thermohaline circulation and vertical mixing: does weaker density stratification give stronger overturning? *J Phys Oceanogr* 33:2781–2795
- Otterå OH, Drange H, Bentsen M et al (2004) Transient response of the Atlantic meridional overturning circulation to enhanced freshwater input to the nordic seas-arctic ocean in the Bergen climate model. *Tellus* 56A:342–361
- Otterå OH, Bentsen M, Bethke I, Kvamstø NG (2009) Simulated pre-industrial climate in Bergen Climate Model (version 2) model description and large-scale circulation features. *Geosci Model Dev* 2:197–212
- Otterå OH, Bentsen M, Drange H, Suo L (2010) External forcing as a metronome for Atlantic multidecadal variability. *Nat Geosci* 3:688–694. doi:[10.1038/NNGEO955](https://doi.org/10.1038/NNGEO955)
- Pèrez-Brunius P, Rossby T, Watts DR (2004) The transformation of the warm waters of the North Atlantic from a stream function perspective. *J Phys Oceanogr* 34:2238–2256
- Peterson BJ, Holmes RM, McClelland JW et al (2002) Increasing river discharge to the Arctic Ocean. *Science* 298:2171–2173
- Pickart RS, Smethie WM Jr, Lazier JRN, Jones EP et al (1996) Eddies of newly formed upper Labrador Sea Water. *J Geophys Res* 101:20711–20726
- Pickart RS, Spall MA, Ribergaard MH et al (2003a) Deep convection in the Irminger Sea forced by the Greenland tip jet. *Nature* 424:152–156
- Pickart RS, Straneo F, Moore GWK (2003b) Is Labrador sea water formed in the Irminger basin? *Deep-Sea Res I* 50:23–52
- Rahmstorf S (1994) Rapid climate transitions in a coupled ocean-atmosphere model. *Nature* 372:82–85
- Rahmstorf S (1996) On the freshwater forcing and transport of the Atlantic thermohaline circulation. *Clim Dyn* 12:799–811
- Rahmstorf S, Ganopolski A (1999) Long-term global warming scenarios computed with an efficient coupled climate model. *Clim Change* 43:353–367
- Rhein M, Stramma L, Send U (1995) The Atlantic Deep Western Boundary Current: water masses and transport near the equator. *J Geophys Res* 100:2441–2457
- Ridley JK, Huybrechts P, Gregory JM, Lowe JA (2005) Elimination of the Greenland ice sheet in a high CO₂ climate. *J Clim* 18:3409–3427
- Rignot E, Koppes MC, Velicogna I (2010) Rapid submarine melting of the calving faces of West Greenland glaciers. *Nat Geosci* 3:187–191

- Rignot E, Velicogna I, van den Broeke MR et al (2011) Acceleration of the contribution of the Greenland and Antarctic ice sheets to sea level rise. *Geophys Res Lett* 38:L05503
- Roche DM, Wiersma AP, Renssen H (2010) A systematic study of the impact of freshwater pulses with respect to different geographical locations. *Clim Dyn* 24:997–1013
- Rooth C (1982) Hydrology and ocean circulation. *Prog Oceanogr* 11:131–149. doi:10.1016/0079-6611(82)90006-4
- Saenko OA, Weaver AJ, Robitaille DY, Flato GM (2007) Warming of the subpolar Atlantic triggered by freshwater discharge at the continental boundary. *Geophys Res Lett* 34:L15604. doi:10.1029/2007GL030674
- Salas-Mélia D (2002) A global coupled sea ice-ocean model. *Ocean Model* 4:137–172. doi:10.1016/S1463.4003(01)00015-4
- Schiller A, Mikolajewicz U, Voss R (1997) The stability of the North Atlantic thermohaline circulation in a coupled ocean-atmosphere general circulation model. *Clim Dyn* 13:325–347
- Sciascia R, Straneo F, Cenedese C et al (2013) Seasonal variability of submarine melt rate and circulation in an East Greenland fjord. *J Geophys Res* 118:2492–2506
- Shepherd A, Ivins ER, Geruo A et al (2012) A reconciled estimate of ice-sheet mass balance. *Science* 338:1183–1189
- Smeed DA, McCarthy GD, Cunningham SA et al (2014) Observed decline of the Atlantic Meridional Overturning Circulation 2004–2102. *Ocean Sci* 10:29–38. doi:10.5194/os-10-29-2014
- Smethie WM Jr, Fine RA, Putzka A, Jones EP (2000) Tracing the flow of North Atlantic Deep Water using chlorofluorocarbons. *J Geophys Res* 105:14297–14323
- Smith RS, Gregory JM (2009) A study of the sensitivity of ocean overturning circulation and climate to freshwater input in different regions of the North Atlantic. *Geophys Res Lett* 36:L15701. doi:10.1029/2009GL038607
- Stommel H (1961) Thermohaline convection with two stable regimes of flow. *Tellus* 13:224–230
- Stouffer RJ, Yin J, Gregory JM, Dixon KW et al (2006) Investigating the causes of the response of the thermohaline circulation to past and future climate changes. *J Clim* 19:1365–1387
- Straneo F, Hamilton GS, Sutherland DA et al (2010) Rapid circulation of warm subtropical waters in a major glacial fjord in East Greenland. *Nature Geosci* 3:182–186
- Suo L, Otterå OH, Bentsen M, Gao Y, Johannessen OM (2013) External forcing of the early 20th century Arctic warming. *Tellus (A)* 65. doi:10.3402/tellusa.v65i0.20578
- Swingedouw D, Rodehacke CB, Behrens E et al (2013) Decadal fingerprints of freshwater discharge around Greenland in a multi-model ensemble. *Clim Dyn* 41(3–4):695–720. doi:10.1007/s00382-012-1479-9
- Terray L, Thuau O, Belamari S et al (1995) Climatology and interannual variability simulated by the ARPEGE-opa model. *Clim Dyn* 11:487–505
- Thomas R, Frederick E, Krabill W, Manizade S, Martin C (2009) Recent changes on Greenland outlet glaciers. *J Glaciol* 55:147–162
- Toom MD, Dijkstra HA, Weijer W et al (2014) Response of a strongly eddying global ocean to North Atlantic freshwater perturbations. *J Phys Oceanogr* 44:464–481
- Tziperman E (2000) Proximity of the present day thermohaline circulation to an instability threshold. *J Phys Oceanogr* 30:90–104
- Våge K, Pickart RS, Moore GWK, Ribergaard MH (2008) winter mixed layer development in the central Irminger Sea: the effect of strong, intermittent wind events. *J Phys Oceanogr* 38:541–565
- Vellinga MR, Wood A, Gregory JM (2002) Processes governing the recovery of a perturbed Thermohaline Circulation in HadCM3. *J Clim* 15:764–780
- Vizcaíno M, Mikolajewicz U, Jungclauss J et al (2010) Climate modification by future ice sheet changes and consequences for ice sheet mass balance. *Clim Dyn* 34:301–324
- Weijer W, Maltrud ME, Hecht MW et al (2012) Response of the Atlantic ocean circulation to Greenland ice sheet melting in a strongly-eddying ocean model. *Geophys Res Lett* 39:L09606. doi:10.1029/2012GL051611
- Yu L, Gao YQ, Wang HJ, Drange H (2008) Revisiting effect of ocean diapycnal mixing on Atlantic meridional overturning circulation recovery in a freshwater perturbation simulation. *Adv Atmos Sci* 25:597–609
- Yu L, Gao YQ, HJ Wang et al (2009) The responses of East Asian summer monsoon to the North Atlantic Meridional Overturning Circulation in an enhanced freshwater input simulation. *Chin Sci Bull* 54:4724–4732. doi:10.1007/s11434-009-0720-3
- Zhang J, Schmitt RW, Huang RX (1999) The relative influence of diapycnal mixing and hydrological forcing on the stability of thermohaline circulation. *J Phys Oceanogr* 29:1096–1108
- Zhang R, Kang SM, Held IM (2010) Sensitivity of climate change induced by the weakening of the Atlantic Meridional Overturning Circulation to cloud feedback. *J Clim* 23:378–389. doi:10.1175/2009JCLI3118.1
- Zhu X, Jungclauss JH (2008) Interdecadal variability of the meridional overturning circulation as an ocean internal mode. *Clim Dyn* 31:731–741